Ising Ferromagnets on Proximity Graphs with Varying Disorder of the Node Placement

Hendrik Schawe[1,*], Christoph Norrenbrock[1], and Alexander K. Hartmann[1]

[1]Institut für Physik, Universität Oldenburg, 26111 Oldenburg, Germany
[*]hendrik.schawe@uni-oldenburg.de

ABSTRACT

We perform Monte Carlo simulations to determine the critical temperatures of Ising Ferromagnets (IFM) on different types of two-dimensional proximity graphs, in which the distribution of their underlying node sets has been changed systematically by means of a parameter σ. This allows us to interpolate between regular grids and proximity graphs based on complete random placement of nodes. Each edge of the planar proximity graphs carries a weighted ferromagnetic coupling. The coupling strengths are determined via the Euclidean distances between coupled spins. The simulations are carried out on graphs with $N = 16^2$ to $N = 128^2$ nodes utilising the Wolff cluster algorithm and parallel tempering method in a wide temperature range around the critical point to measure the Binder cumulant in order to obtain the critical temperature for different values of σ. Interestingly, the critical temperatures depend partially non-monotonously on the disorder parameter σ, corresponding to a non-monotonous change of the graph structure. For completeness, we further verify using finite-size scaling methods that the IFM on proximity graphs is for all values of the disorder in the same universality class as the IFM on the two-dimensional square lattice.

1Introduction

The Ising model of ferromagnetism[1] is one of the most extensively studied models in statistical mechanics, because it features a continuous phase transition while being simple. The model consists of spins, which can be in one of two different states "+1" and "-1". The pair-wise interactions of spins, can be expressed by graphs and thus there is a constant interest in the critical behaviour of this model on different graph ensembles. The research provides the whole range from analytical results for regular lattices[2,3] to numerical results for complex networks.[4,5,6,7]

An important type of graph is obtained from the Delaunay triangulation that finds application in, e.g., finite volume methods.[16,17] For a system of randomly placed Ising spins on a two-dimensional surface with neighbour relationships derived from a Delaunay triangulation, the critical temperature has been obtained and it has been confirmed that it is in the same universality class, as the two-dimensional Ising model on a square lattice[18,19]

The availability of results for this special case motivated us to extend and generalise the former research in two ways: First, we study two other types of irregular lattices, namely the *Relative Neighborhood graph* (RNG)[22] and *Gabriel graph* (GG),[23] which are subgraphs of the Delaunay triangulation[24] and belong to the family of *proximity graphs*. The objective of proximity graphs is to connect nodes which are spatially close to each other, hence they are suited to generalise problems defined on regular lattices with nearest neighbour relationships. This family of graphs finds application in geographic variation studies in biology,[25,26,27] as potential candidates for "virtual backbones" in ad-hoc networks[28,29,30,31,32] and in machine learning and pattern recognition.[33] Also, their statistical properties have been under scrutiny recently.[34,35]

As a second generalisation and extension, we consider an ensemble of node sets depending on a tunable parameter σ. By changing this parameter we can interpolate the configurations between a square lattice and nodes distributed by a Poisson point process. A similar approach has recently been used[36] to introduce an ensemble of Travelling Salesperson Problems (TSP) which interpolates between an easy to solve circular arrangement and a hard to solve random placement of the nodes.

For any node set the construction rule of a proximity graph defines the corresponding edge set. Thus, the parameter σ influences the regularity of the resulting proximity graph. Below, we measure the critical temperatures for a range of σ. Additionally, , we verify by applying a common finite-size scaling analysis and by considering the two-point finite-size correlation function that the universality class does not depend on the graph type and does not change when varying σ.

The remainder of this work is organised as follows: First the RNG, GG and the Ising model are introduced. Then the details and results of our simulations are discussed.At the end a conclusion of this article is given.

1Model

1Proximity Graphs

An *undirected graph* $G(V,E)$ consists of a set of nodes V and edges $E \subset V^{(2)}$. Two nodes connected by an edge are called *neighbours*. Proximity graphs are defined in a metric space. In this article a two-dimensional space with Euclidean metric is chosen, because it is the most common case and easy to visualise. Though every metric in any dimension can be used, in principle.

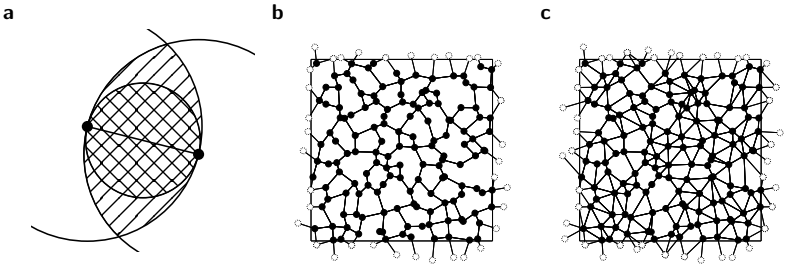

Figure 1. (**a**) Lunes of two nodes regarding the RNG (hatched region) and GG (cross hatched region), respectively. If there is no node located in the lune, both depicted nodes will be linked by an edge. (**b**) Example of the RNG with periodic boundary conditions. (**c**) Example of the GG with periodic boundary conditions. Mirror images of nodes (visualising the periodic boundary conditions) are shown in white.

One of the proximity graphs we consider here is the *Relative Neighbourhood graph* (RNG).[22] Within this graph two nodes i and j with distance d_{ij} will be connected, if no other node is located in a well defined area called *lune*. The lune is defined as the intersection area of two disks with radius $r = d_{ij}$, whose centres are on node i and j, respectively. This means that the edge $\{i, j\}$ will be part of the RNG, if the condition

$$d_{ij} \leq \max\left\{d_{ik}, d_{kj}\right\} \quad \forall k \in V \setminus \{i, j\}$$

is fulfilled. For the sake of clarity the lune of two nodes in regard to the RNG is sketched in Fig. 1a (hatched region). An example of the RNG is given in Fig. 1b. For a Poisson point process in a square, i.e., nodes placed on uniformly distributed, independent coordinates, its mean degree is $K = 2.5576(3)$,[34] i.e., the mean number of neighbours of each node.

The second proximity graph we study is the *Gabriel graph* (GG).[23] In the GG two nodes i and j with distance d_{ij} will be connected, if the disk which has the connecting line between i and j as its diameter contains no further nodes $k \in \{i, j\}$, i.e., the condition

$$d_{ij}^2 < d_{ik}^2 + d_{kj}^2 \quad \forall k \in V \setminus \{i, j\}$$

is fulfilled. The lune is illustrated in Fig. 1a (cross hatched region). An example of the GG is given in Fig. 1c. Note that the lune of the GG is completely enclosed in the lune of the RNG, therefore the RNG is a subgraph of the GG and, as a consequence, all edges belonging to the RNG also belong to the GG. For a Poisson point process in a square, its mean degree is $K = 4$[35] – the same as the square lattice. Note that by construction RNG and GG have no crossing edges, i.e., they are *planar*. Furthermore they are *connected*, i.e., consist only of one connected component.

For any given set of nodes located in a two-dimensional plane these graphs can be constructed by an algorithm[34] featuring a time complexity of $\mathcal{O}(N \log N)$. In this algorithm the Delaunay Triangulation, which can be constructed in $\mathcal{O}(N \log N)$[38] and which is a supergraph of the RNG and GG, is obtained first. Subsequently its edges, of which there are $|E| = \mathcal{O}(N)$, are checked in regard to the aforementioned construction rules.

A simple construction of proximity graphs can be based on a uniform and random placement of nodes. To allow for a more complex behaviour, we apply a more general approach. Here, first the $N = L^2$ nodes are placed to form a regular square lattice with periodic boundary conditions. Next, the nodes are *displaced*, introducing geometric disorder resulting in a non-regular graph structure. The horizontal displacement Δx and vertical displacement Δy of each node is drawn from a Gaussian distribution with zero mean and standard deviation σ. Therefore, via the parameter σ we are able to interpolate between fully regular and fully random placement. The influence of σ on the structure of a proximity graph has two main effects which are clearly visible in Fig. 2 for the RNG. First, the number of edges changes as will be examined in more detail later on (see Fig. 4b). Second, the variance of the length of the edges increases, i.e., there are some quite long and some very short edges in configurations with increasing σ.

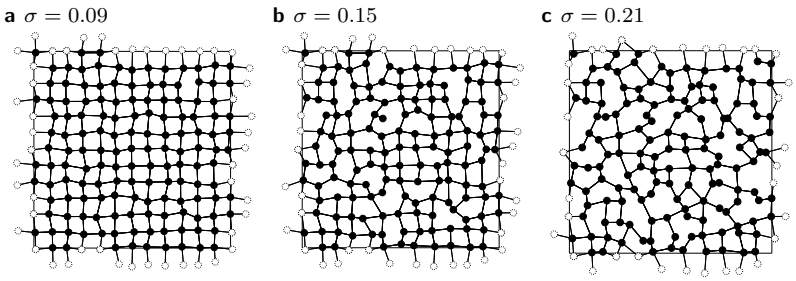

Figure 2. (**a**) - (**c**) Examples of proximity graphs (more precisely, RNG) for different values of σ. Connections which cross a periodic boundary are indicated by edges which connect a black node to a white node.

1The Ising Model

Commonly, the IFM is studied on a square lattice with lateral length L and $N = L^2$ nodes with periodic boundary conditions. Each node i has an Ising spin $s_i \in \{-1, +1\}$ and interacts with its neighbours according to the Hamiltonian

$$\mathscr{H} = -\sum_{\langle i,j \rangle} J_{ij} s_i s_j.$$

$\langle i, j \rangle$ refers to nodes i and j which are nearest neighbours, i.e., they are connected by an edge. The coupling strength between i and j is given by J_{ij}.

In the generalised graph we use here, the interaction structure is not regular. To account for the varying distances, we choose the coupling constants J_{ij}, which depend on the geometric distance between the connected pair of nodes. More precisely, the coupling constant of an edge $\{i, j\}$ is

$$J_{ij} = \mathrm{e}^{\alpha(1-d_{ij})},$$

where d_{ij} is the Euclidean distance between node i and j. Following the work of Lima et al.[19] the free parameter α is set to $\alpha = 0.5$. Note that distances smaller and larger than one can appear. For $\sigma = 0$ all $d_{ij} = 1$ and therefore all $J_{ij} = 1$ for every edge $\{i, j\} \in E$.

1Results

The results were obtained through Monte Carlo simulations at different temperatures. For each realisation of a graph, at each temperature independent configurations were simulated. For a *sweep* for all configurations $N = L^2$ single spin flip Metropolis attempts[39] plus one Wolff cluster update[40] was performed. To speed up equilibration, we allowed the configurations to change temperatures in a controlled way via applying the Metropolis-Coupled Markov Chain Monte Carlo (MCMCMC) method,[41] also known as Parallel Tempering.[42,43] Thus, within one sweep an exchange of the configurations between a randomly chosen pair of neighbouring temperatures was attempted. Since it is not known beforehand, where the critical temperatures T_c are located, the Wolff cluster algorithm is used at every temperature. This combination of single-spin flip sweeps and Wolff steps guarantees for a *convenient* and rather fast equilibration and decorrelation at any temperature. Albeit the efficiency of the algorithmic procedure was not examined for every temperature, the speed up near criticality should be worth the moderate slow down at other temperatures.

For every system size $L \in \{16, 32, 64, 128\}$ 19 different values of $\sigma \in [0, 1.2]$ were considered. To average over the disorder, 100 different realisations are simulated for each system size L and disorder strength σ. Every realisation was simulated at about a hundred different temperatures $T \in [0.1, 3.3]$ until at least 5000 independent measurements in equilibrium were obtained to get the thermal average, which needed up to 160000 sweeps.

1Reproduction of the Critical Exponents

First, we want to confirm that the Ising model on both planar proximity graphs belong to the same universality class as the Ising model on a square lattice. This can be since $d\nu = 2$ for the Ising model and therefore, according to the Harris criterion,[21] the disorder is not relevant, or at least border-line, i.e., its influence is hard to detect.[44] Therefore not only the critical exponents were obtained, but also a sensitive test using the two-point finite-size correlation function was done. The critical exponents

were determined by a finite-size scaling (FSS) analysis.[45] Therefore we looked at the magnetisation m, susceptibility χ and Binder cumulant g, which are defined as

$$m = \frac{1}{N}\sum_i s_i,$$
$$\chi = \frac{N}{T}\left[\langle m^2\rangle - \langle m\rangle^2\right]_{\text{avg}},$$
$$g = \frac{3}{2}\left[1 - \frac{\langle m^4\rangle}{3\langle m^2\rangle^2}\right]_{\text{avg}}.$$

Here, $\langle\ldots\rangle$ denotes the thermal average and $[\ldots]_{\text{avg}}$ the average over the disorder realisations. For all quantities, we obtained statistical errors via bootstrapping.[46,47]

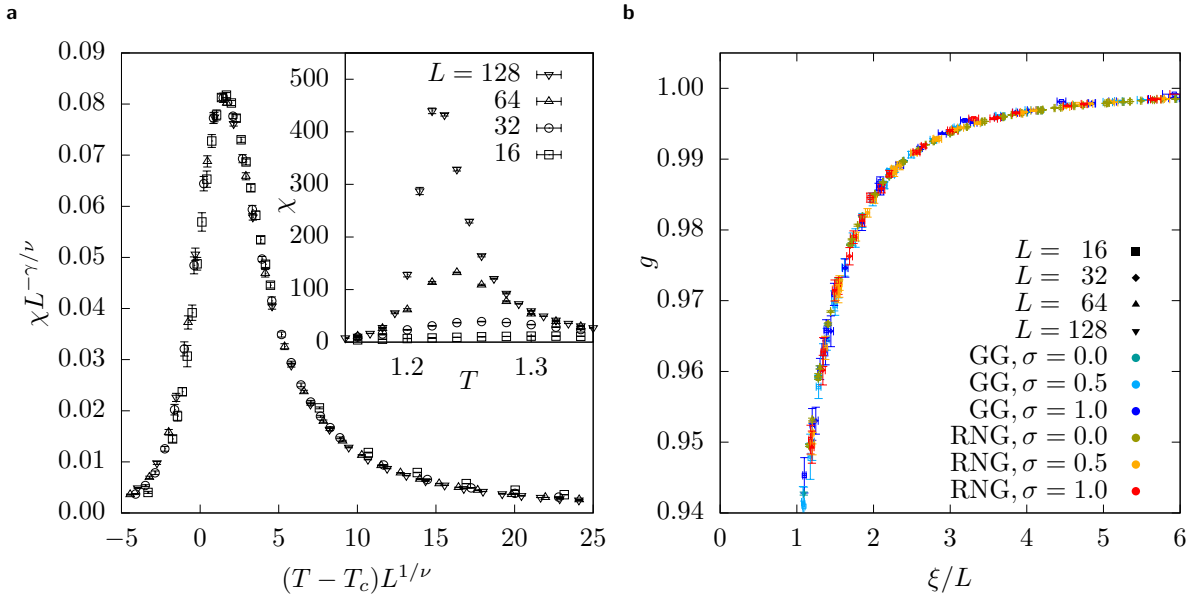

Figure 3. (**a**) Example of a data collapse of the susceptibility χ in regards to the RNG at $\sigma = 1$ to get the corresponding critical exponent γ. The same procedure is used on the Binder cumulant g and the magnetisation $|m|$ to determine the critical exponents ν and β and the critical temperature T_c. The inset shows the same data with unscaled axes. (**b**) Binder cumulant g as a function of the two-point finite-size correlation function divided by system size L. The data points for different system sizes are drawn with different symbols, while the data points for different graph ensembles are drawn with different shades of grey (colors online). All points fall on one curve within errorbars.

We determine the exponents by using the finite-size scaling assumption[48,49] for phase transitions of 2nd order, e.g., for the susceptibility χ:

$$\chi_L = L^{\gamma/\nu}\tilde{C}(L^{1/\nu}(T - T_c)),$$

where $\tilde{C}(\cdot)$ is some unknown scaling function. That means, for the right choice of ν, γ and T_c and appropriately scaled axes, the measurements at different system sizes L collapse on the scaling function as shown in Fig. 3a. A similar formula is valid for m (containing β) and g (which is dimensionless, i.e., has no prefactor in front of the scaling function). Values for the exponents and T_c are obtained in an automated and reproducible way.[50] They are visualised in Tab. 1 and are within errorbars consistent with the exactly known values for the square lattice IFM.

A more sensitive method[51,52] to test whether two models are in the same universality class includes the analysis of the two-point finite-size correlation function

$$\xi = \frac{1}{2\sin\left(\left|\vec{k}_{\min}\right|/2\right)}\sqrt{\frac{\chi(\vec{0})}{\chi(\vec{k}_{\min})} - 1}$$

where $\vec{k}_{\min} = (2\pi/L, 0)$ and $\chi(\vec{k})$ is the wave vector dependent susceptibility

$$\chi(\vec{k}) = \left[\left\langle \left| \left(\frac{1}{N} \sum_j s_j \exp(ikx_j) \right)^2 \right| \right\rangle \right]_{\text{avg}},$$

which is in this case only evaluated over one direction, thus x_j is the position of the node in the horizontal direction.

We have plotted the Binder cumulant g as a function of ξ/L for different values of σ, L and T as shown in Fig. 3b. We can observe that within error bars all data points fall on the same curve, which confirms that the universality class does not change by varying σ.

1Behaviour of the Critical Temperature

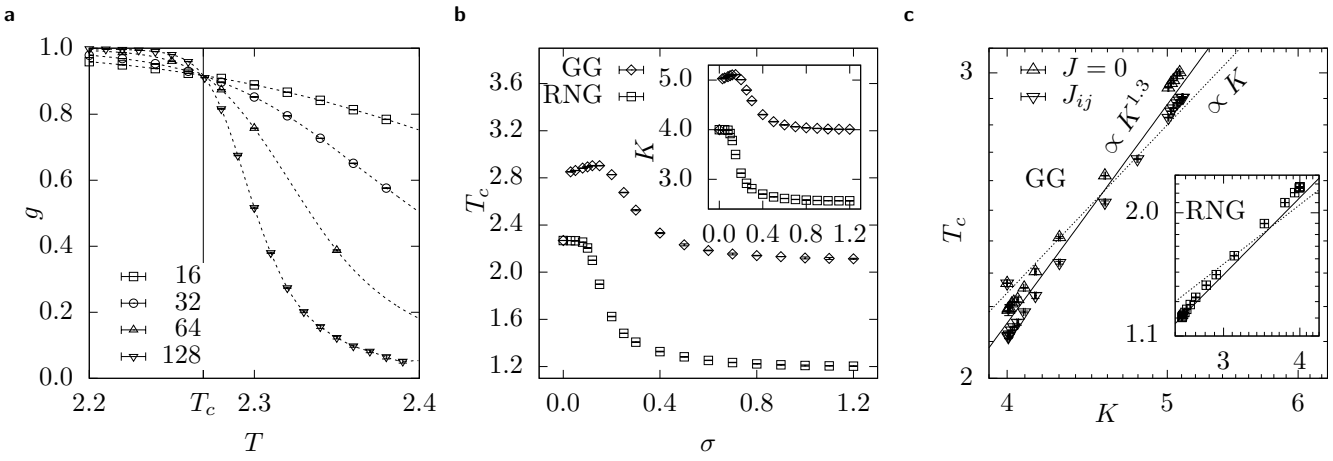

Figure 4. (**a**) Critical temperatures T_c are obtained by finding the intersections of the Binder cumulants g for different system sizes L. (**b**) T_c as a function of σ. The inset shows the average degree K as a function of σ. (**c**) T_c as a function of K on a log-log scale.

This study examines the critical temperatures T_c for different values of σ. In order to locate T_c we considered the Binder cumulants for different system sizes L, because they are intersecting at the critical point T_c[53] as shown in Fig. 4a. Since g is only measured for discrete values of T, the points have to be interpolated to find the intersection. Therefore a *cubic spline*[54] interpolation is calculated for the measured points. An even better method would be the *multiple histogram* method.[55,43] But the simple cubic spline interpolation seems to deliver results that are good enough,

In Fig. 4b the critical temperatures are shown as a function of the disorder strength. Interestingly, we first observe that for the GG there occurs a jump from $T_c(0) = 2.2690(3)$ to a value close to the measured value $T_c(0.03) = 2.8511(7)$. This is easily explainable, because the square lattice at $\sigma = 0$ is a very special case for the GG. At very small deviations from the square lattice new edges arise in the GG, this is visualised in Fig. 5a-c. These new edges lead to a stronger coupling of spins such that the system stays ferromagnetic at higher temperatures. After an initial increase of the GG's critical temperature with growing disorder, a maximum is reached and the critical temperature drops. Thus, the dependence is non-monotonous. This can be understood when analysing the dependence of the average number K of neighbours as a function of the disorder strength σ, as shown in Fig. 4b. The behaviour of T_c and K is very similar: $K(\sigma)$ exhibits also a jump at $\sigma = 0$ as well as a peak close to $\sigma = 0.2$. This is confirmed when plotting T_c as a function of K, see Fig. 4c. Note that the $\sigma = 0$ point is not part of this power law, which is expected, since it is a special corner case as mentioned above.

For large values of σ the node configurations approach the limit of a Poisson point process, hence T_c approaches a limit value, which was obtained from a fit as $T_c(\sigma = \infty) = 2.10(3)$ for the GG and $T_c(\sigma = \infty) = 1.19(1)$ for the RNG. A further interesting feature which highlights the importance of the structure of the graph for the critical temperature is the fact that the square lattice has a slightly different critical temperature than the GG in the Poisson point process limit although they share the same average degree $K = 4$.[35]

For the RNG, the critical temperature T_c of the RNG decreases smoothly and monotonously with increasing value σ. Therefore, the RNG exhibits neither a jump at $\sigma = 0$ nor a peak. This is reflected by the behaviour of $K(\sigma)$ originating from a decrease of the number of edges, see Fig. 2 and Fig. 4b. Note also that for the RNG the power law between critical temperature and number of neighbours is well visible and

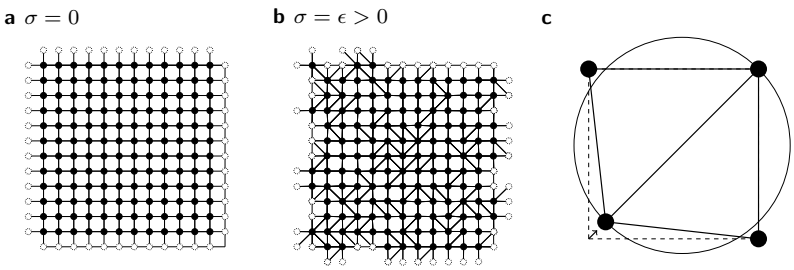

Figure 5. Visualisation of the occurence of the Jump at small values of σ for the GG. (**a**) The regular lattice with no disorder. (**b**) Example of a graph for a very small value of the disorder. (**c**) Sketch of a GG with $N = 4$ nodes for very small σ. Due to the construction rule of the GG a new edge appears resulting in a jump in K and T_c, see Fig. 4b. This does not occur in the RNG.

1Conclusion

We have performed Monte Carlo simulations of an Ising Ferromagnet in a two-dimensional Euclidean plane with neighbour relationships defined by two different proximity graphs, the Relative Neighbourhood graph and Gabriel graph. Controlled by a disorder parameter σ we can smoothly interpolate between a regular square lattice node arrangement and a completely random node arrangement.

By means of finite-size scaling analysis and by studying the two-point finite-size correlation function, we confirmed the expectation that the universality class does not change for different graph types and for different values of σ. Furthermore, we have monitored the critical temperature T_c as a function of σ. For GG we observe a jump and a non-monotonous behaviour, reflecting non-trivial changes of the graph topology. On the other hand, for RNG, T_c stays approximately constant for small values of σ and decreases to some limit value for large disorder. In fact, T_c strongly depends on the degree K. It turns out that there is a power-law relationship between T_c and K for . Even if the degree $K = 4$ of the GG at $\sigma = 0$ is equal to the degree for large values of σ, the critical temperature is lower at this point. Therefore, it becomes obvious that the average number of interaction partners is the dominating but not the sole influence for the location of the critical point.

1References

1. Ising, E. Beitrag zur Theorie des Ferromagnetismus. *Zeitschrift für Physik* **31**, 253 (1925).
2. Onsager, L. Crystal statistics. i. a two-dimensional model with an order-disorder transition. *Phys. Rev.* **65**, 117–149 (1944).
3. Wannier, G. H. The statistical problem in cooperative phenomena. *Rev. Mod. Phys.* **17**, 50–60 (1945).
4. Aleksiejuk, A., Hołyst, J. A. & Stauffer, D. Ferromagnetic phase transition in Barabási–Albert networks. *Physica A: Statistical Mechanics and its Applications* **310**, 260 – 266 (2002).
5. Herrero, C. P. Ising model in small-world networks. *Phys. Rev. E* **65**, 066110 (2002).
6. Herrero, C. P. Ising model in scale-free networks: A Monte Carlo simulation. *Phys. Rev. E* **69**, 067109 (2004).
7. Herrero, C. P. Ising model in clustered scale-free networks. *Phys. Rev. E* **91**, 052812 (2015).
8. Lima, F. & Plascak, J. Critical behavior of the Ising and Blume-Capel models on directed two-dimensional small-world networks. *The European Physical Journal B* **86**, 300 (2013).
9. Malmi-Kakkada, A. N., Valls, O. T. & Dasgupta, C. Ising model on a random network with annealed or quenched disorder. *Phys. Rev. B* **90**, 024202 (2014).
10. Sumour, Muneer A. & Lima, F. W. S. Unusual ferromagnetism in Ising and Potts model on semi-directed Barabási-Albert networks. *Eur. Phys. J. Plus* **129**, 127 (2014).
11. Sousa, E. M. & Lima, F. W. S. Ising model on directed small-world Voronoi Delaunay random lattices. *The European Physical Journal Plus* **128**, 150 (2013).
12. Carro, A., Toral, R. & San Miguel, M. The noisy voter model on complex networks. *Scientific reports* **6** (2016).
13. Lima, F. W.S., Costa, U. M.S., Almeida, M. P. & Andrade, J. S. Critical behavior of a three-state Potts model on a Voronoi lattice. *Eur. Phys. J. B* **17**, 111–114 (2000).

14. Reichardt, J. & Bornholdt, S. Detecting fuzzy community structures in complex networks with a Potts model. *Phys. Rev. Lett.* **93**, 218701 (2004).

15. Son, S.-W., Jeong, H. & Noh, J. D. Random field Ising model and community structure in complex networks. *The European Physical Journal B - Condensed Matter and Complex Systems* **50**, 431–437 (2006).

16. Ho-Le, K. Finite element mesh generation methods: a review and classification. *Computer-aided design* **20**, 27–38 (1988).

17. Mishev, I. D. Finite volume methods on voronoi meshes. *Numerical methods for Partial Differential equations* **14**, 193–212 (1998).

18. Janke, W., Katoot, M. & Villanova, R. Single-cluster Monte Carlo study of the Ising model on two-dimensional random lattices. *Phys. Rev. B* **49**, 9644–9657 (1994).

19. Lima, F., Moreira, J., Jr., J. A. & Costa, U. The ferromagnetic Ising model on a Voronoi–Delaunay lattice. *Physica A: Statistical Mechanics and its Applications* **283**, 100 – 106 (2000).

20. Lima, F., Costa, U. & Filho, R. C. Critical behavior of the 3d Ising model on a poissonian random lattice. *Physica A: Statistical Mechanics and its Applications* **387**, 1545 – 1550 (2008).

21. Harris, A. B. Effect of random defects on the critical behaviour of Ising models. *J. Phys. C* **7**, 1671 (1974).

22. Toussaint, G. The relative neighbourhood graph of a finite planar set. *Pattern Recognition* **12**, 261–268 (1980).

23. Gabriel, K. R. & Sokal, R. R. A new statistical approach to geographic variation analysis. *Systematic Biology* **18**, 259–278 (1969).

24. Delaunay, B. N. Sur la sphère vide. *Bulletin of Academy of Sciences of the USSR* 793–800 (1934).

25. Sokal, R. R. & Oden, N. L. Spatial autocorrelation in biology: 1. methodology. *Biological Journal of the Linnean Society* **10**, 199–228 (1978).

26. Sokal, R. R., Bird, J. & Riska, B. Geographic variation in pemphigus populicaulis (insecta: Aphididae) in eastern north america. *Biological Journal of the Linnean Society* **14**, 163–200 (1980).

27. Selander, R. K. & Kaufman, D. W. Genetic structure of populations of the brown snail (helix aspersa). i. microeographic variation. *Evolution* **29**, 385–401 (1975).

28. Kuhn, F., Wattenhofer, R. & Zollinger, A. Ad-hoc networks beyond unit disk graphs. In *Proceedings of the 2003 joint workshop on Foundations of mobile computing*, DIALM-POMC '03, 69–78 (ACM, New York, NY, USA, 2003).

29. Bose, P., Morin, P., Stojmenović, I. & Urrutia, J. Routing with guaranteed delivery in ad hoc wireless networks. *Wirel. Netw.* **7**, 609–616 (2001).

30. Santi, P. Topology control in wireless ad hoc and sensor networks. *ACM Comput. Surv.* **37**, 164–194 (2005).

31. Karp, B. & Kung, H.-T. Gpsr: greedy perimeter stateless routing for wireless networks. In *Proceedings of the 6th annual international conference on mobile computing and networking*, 243–254 (ACM, 2000).

32. Jennings, E. & Okino, C. Topology control for efficient information dissemination in ad-hoc networks. In *International Symposium on Performance Evaluation of Computer and Telecommunication Systems SPECTS*, vol. 2002 (Citeseer, 2002).

33. Bhattacharya, B. K., Poulsen, R. S. & Toussaint, G. T. Application of proximity graphs to editing nearest neighbor decision rule. In *International Symposium on Information Theory, Santa Monica* (1981).

34. Melchert, O. Percolation thresholds on planar Euclidean relative-neighborhood graphs. *Phys. Rev. E* **87**, 042106 (2013).

35. Norrenbrock, C. Percolation threshold on planar euclidean Gabriel graphs. *The European Physical Journal B* **89**, 1–6 (2016).

36. Schawe, H. & Hartmann, A. K. Phase transition of traveling salesperson problems solved with linear programming and cutting planes. *Eur. Phys. Lett.* **113**, 30004 (2016).

37. Katsura, S. & Takizawa, M. Bethe lattice and the Bethe approximation. *Progress of Theoretical Physics* **51**, 82–98 (1974).

38. Katajainen, J. & Nevalainen, O. Computing relative neighbourhood graphs in the plane. *Pattern Recognition* **19**, 221–228 (1986).

39. Metropolis, N., Rosenbluth, A. W., Rosenbluth, M. N., Teller, A. H. & Teller, E. Equation of state calculations by fast computing machines. *The Journal of Chemical Physics* **21**, 1087–1092 (1953).

40. Wolff, U. Collective Monte Carlo updating for spin systems. *Phys. Rev. Lett.* **62**, 361–364 (1989).

41. Geyer, C. Monte Carlo maximum likelihood for depend data. In *23rd Symposium on the Interface between Computing Science and Statistics*, 156 (Interface Foundation North America, Fairfax, 1991).

42. Hukushima, K. & Nemoto, K. Exchange Monte Carlo method and application to spin glass simulations. *J. Phys. Soc. Jpn.* **65**, 1604 (1996).

43. Newman, M. E. J. & Barkema, G. T. *Monte Carlo Methods in Statistical Physics* (Oxford University Press, USA, 1999).

44. Mazzeo, G. & Kühn, R. Critical behavior of the two-dimensional spin-diluted Ising model via the equilibrium ensemble approach. *Phys. Rev. E* **60**, 3823–3836 (1999).

45. Binder, K. & Heermann, D. W. *Monte Carlo Simulation in Statistical Physics* (Springer, 2010).

46. Efron, B. Bootstrap methods: Another look at the jackknife. *Ann. Statist.* **7**, 1–26 (1979).

47. Hartmann, A. K. *Big Practical Guide To Computer Simulations* (World Scientific Publishing Company, Incorporated, Singapore, 2015).

48. Cardy, J. *Finite-size Scaling* (Elsevier, Amsterdam, 1988).

49. Goldenfeld, N. *Lectures on phase transitions and the renormalization group* (Addison-Wesely, Reading (MA), 1992).

50. Melchert, O. autoscale.py - a program for automatic finite-size scaling analyses: A user's guide (2009). ArXiv:0910.5403 [physics.comp-ph].

51. Katzgraber, H. G., Körner, M. & Young, A. P. Universality in three-dimensional Ising spin glasses: A Monte Carlo study. *Phys. Rev. B* **73**, 224432 (2006).

52. Ahrens, B., Xiao, J., Hartmann, A. K. & Katzgraber, H. G. Diluted antiferromagnets in a field seem to be in a different universality class than the random-field Ising model. *Phys. Rev. B* **88**, 174408 (2013).

53. Binder, K. Critical properties from Monte Carlo coarse graining and renormalization. *Phys. Rev. Lett.* **47**, 693–696 (1981).

54. Press, W. H. *Numerical recipes 3rd edition: The art of scientific computing* (Cambridge university press, 2007).

55. Ferrenberg, A. M. & Swendsen, R. H. Optimized Monte Carlo data analysis. *Physical Review Letters* **63**, 1195 (1989).

56. Pelissetto, A. & Vicari, E. Critical phenomena and renormalization-group theory. *Physics Reports* **368**, 549 – 727 (2002).

1Acknowledgements

The simulations were performed at the HPC Cluster HERO, located at the University of Oldenburg (Germany) and funded by the DFG through its Major Research Instrumentation Programme (INST 184/108-1 FUGG) and the Ministry of Science and Culture (MWK) of the Lower Saxony State. The authors would also like to thank O. Melchert for stimulating discussions.

1Author contributions statement

C.N. and A.K.H. conceived the project, H.S. developed the code, conducted the simulations and analysed the results in consultation with C.N. and A.K.H. All authors contributed to the manuscript.

1Additional information

Competing financial interests The authors declare no competing financial interests.

Table 1. Critical exponents for different values of σ. A finite size scaling analysis was performed to determine the critical exponents β, γ, ν and the critical temperature T_c. The errors for β and γ are estimated with the method from by an iterative method[50]. The errors of ν and T_c are the standard deviation of three obtained values through different collapses. The critical exponents are in reasonable agreement with the exact known values for the 2D Ising universality class. The critical temperatures T_c are shifting as expected.

	σ	T_c	ν	γ	β
exact[56]	0	2.2691...	1	1.75	0.125
RNG	0.0	2.2688(7)	1.00(1)	1.74(1)	0.125(1)
	0.1	2.2053(6)	0.99(1)	1.75(1)	0.128(3)
	0.2	1.6265(19)	1.02(2)	1.76(1)	0.122(7)
	0.5	1.2825(9)	1.01(2)	1.75(2)	0.128(8)
	1.0	1.2125(5)	1.01(1)	1.76(1)	0.125(6)
GG	0.0	2.2688(6)	1.00(1)	1.74(2)	0.127(4)
	0.1	2.8944(43)	1.00(1)	1.75(1)	0.135(6)
	0.3	2.5281(27)	1.03(3)	1.72(2)	0.118(11)
	0.5	2.2388(9)	1.01(1)	1.75(1)	0.125(11)
	1.0	2.1275(20)	1.04(3)	1.75(2)	0.125(15)